CHAPTER 4

System Identification

The process of system identification in structural engineering can be understood as identifying parameters for a numerical model that best represents the measured response of an instrumented structure (Eykhoff 1974). However, solving for these parameters is often an ill-conditioned inverse problem, making it extremely challenging in its application. Other complications in system identification include the choice of numerical algorithms and models, the amount of available instrumentation, the variability in construction methods and material strength, and any other environmental factors. Typically, system identification employs a least-squares metric to quantify the data fit between the measured response and the model. Specifics vary depending on the construction of the objective function, but one aims to find the minimum of the objective function and thus minimize the least-squares-error.

Lower least-squares-errors mean a better data fit. However, this does not always translate to better model predictions for future responses, since the method may over-fit the measured response. For example, observe a high-degree polynomial data fit that is present in any curve fitting toolbox. A ten-degree polynomial will result in a smaller error compared to a linear fit of the empirical data, but it does not necessarily lead to a better

predictive model, especially when the data demonstrate a roughly linear relationship between the two parameters. This over-fitting of what is likely just noise can easily happen when the chosen model has significantly more parameters relative to the information in the data set.

The over- and under-fitting of data complicate the fidelity of resulting models. To minimize these effects, engineers strive to uncover the underlying structural mechanics that produce these data. Since physical behaviors of structures are difficult to extract from time records alone, experimental setups are needed to complete the picture. However, selecting the right model is open to interpretation; models only perform as well as how an engineer thinks the physical system behaves. Therefore, predictions of responses are only as good as the predictive capability of the model, regardless of the accuracy of previous data fits.

The byproduct of leaving the model selection to an engineer's interpretation is that there is often a number of models developed for the same purpose. In modeling wood-frame structures and subassemblies, each researcher often proposes a proprietary element that mimics the hysteretic behavior of wood-frame construction (Foliente 1994). The objective of this dissertation is not to assess which custom hysteretic element works best (as each has its own advantage), but to provide a methodology to evaluate the results. Chapter 6 will discuss in detail the non-linear numerical model used to model the responses. The remainder of this chapter will focus on linear analysis and identify key modal parameters for the records.

4.1 Linear Analysis

Although it seems counterintuitive to use linear analysis in dealing with responses that can be nonlinear, there are many benefits from using this approach (Beck and Jennings 1980).

When a system is linearized, several fundamental properties can be utilized, such as the principle of superposition, linear elasticity, homogeneity in materials, and conventional computational methods (Ma 1995). The analysis becomes less computationally intensive and easier to comprehend for presentation. Results can be summed up with a few numbers pertaining to the fundamental frequencies, modeshapes, and damping ratios.

Even though linear analysis has been extensively studied and applied, it is still necessary to spend extra effort in interpreting the results. A thorough understanding and application of linear analysis to a system does not equate to knowledge of the governing dynamics of the actual system. This does not mean that the results of linear analysis are not meaningful. Observations of the time-varying trends of the modal parameters can give insights to the nonlinear behavior of the system. These findings will be discussed later in the chapter after an introduction of the linear analysis used for system identification.

4.2 MODE-ID

There are numerous system identification algorithms available for structural analysis. However, not all of them are suitable for strong motion records and nonlinear responses. Many of these methods have severe limitations on signal-to-noise ratio, construction of mass and stiffness matrices (K.-Y. Chen 2003), and geometric information. They also make assumptions that are not suitable for high amplitude transient signals found in an earthquake (He et al. 2005). Some of the methods are ad-hoc, requiring special conditions not met in practice with real seismic response records (James, Carne and Lauffer 1993). Other methods require assumptions that require specific tailoring of the records. This dissertation does not attempt to determine the best method, as an extensive study of all the algorithms is out of the scope of the project (Jovanovie 1997; Asmussen 1997; Sain and

Spencer 2005; Shi 2007; Gang). For purposes of this dissertation, MODE-ID is the method of choice which has its origins in Beck (1978). There are several reasons MODE-ID is used for the system identification routine.

1) Previous results are calculated from MODE-ID (Camelo, Beck and Hall 2002). Using the same algorithm for new data analyses facilitates comparisons.
2) System identification can be performed in the time domain without the need to develop a structural model by constructing mass, stiffness and damping matrices (Beck 1978).
3) MODE-ID can handle linear and nonlinear, multiple input-output, and output-only responses (Beck and Jennings 1980; Werner, Beck and Levine 1987).
4) MODE-ID analysis can be applied on both full and windowed records.
5) Parameter values estimated by MODE-ID can be considered as *most probable values* based on the given data in a Bayesian probability framework (Beck 1990).

Inputs for MODE-ID include ground excitation records, measured structural response histories, and initial modal estimates. The modal parameters estimated for each mode are frequency, damping factor, normalized modeshape, participation factors, initial displacement, and initial velocity. MODE-ID has been applied extensively to earthquake and other dynamic data, demonstrating its robustness. The data fitting in MODE-ID is based on a nonlinear least-squares output-error method. The measure of fit between recorded and calculated responses is optimized by a modal minimization algorithm (Beck

and Beck 1985). Although the minimization is performed in the time domain, a frequency domain MODE-ID can be employed through Parseval's Inequality.

The specifics of the modal identification process are to minimize a measure-of-fit parameter J, defined as the ratio of the mean-square output error between measured and model motions to the mean-square output from the measured motions (Werner, Nisar and Beck 1992). This modal minimization routine first begins with modal decomposition, allowing the response of the structure to be expressed as a superposition of the responses of several single-degree-of-freedom (SDOF) oscillators. Given *N* measurements (N_{in}: base accelerations, N_{out}: floor accelerations) a modal model can be mathematically expressed as

$$\ddot{x}_i = \sum_{m=0}^{M} \ddot{x}_{im}(t), \qquad i = 1,2,\dots,N_{out} \tag{4-1}$$

where *M* is the number modes considered for the model. The *i*th predicted acceleration time history $\ddot{x}_i$ can then be represented as a summation of modal mode responses $\ddot{x}_{im}$. The subscript refers to the contribution of the *m*th mode to the *i*th output channel. For each of the *m* modes, the governing equation is the following:

$$\ddot{x}_{im} + 2\xi_m\omega_m\dot{x}_{im} + \omega_m^2 x_{im} = \phi_{im}\sum_{k=1}^{N_{in}} P_{mk}f_k(t) \tag{4-2}$$

$$x_{im}(0) = \phi_{im}c_m\,, \qquad \dot{x}_{im}(0) = \phi_{im}d_m \tag{4-3}$$

ω_m : natural frequency of *m*th mode

ζ_m : critical damping ratio of *m*th mode

φ_{im} : modeshape component of *m*th mode at the *i*th location

P_{mk} : participation factor of the *m*th input channel for the *m*th mode

c_m : initial modal displacement of *m*th mode

d_m : initial modal velocity of *m*th mode

MODE-ID's modal identification routine can also account for a pseudo-static component by incorporating a pseudo-static matrix that directly relates the input and output channels. Completing the modal decomposition and establishing the time-stepping algorithm (Beck and Dowling 1988), modal minimization determines the combination of parameters $\underline{\theta}$ that minimizes the aforementioned measure of fit J. Given measurement records $\hat{y}_i$, the mean-squared fractional error J can be calculated as the following:

$$J(\underline{\theta}) = \sum_{i=1}^{N_{out}} \sum_{n=1}^{N} [\hat{y}_i(n) - \ddot{x}_i(n;\underline{\theta})]^2 \tag{4-4}$$

MODE-ID performs a series of sweeps in which optimization is performed one mode at a time. Optimization within each mode is calculated by the method of steepest descent with respect to the modal frequency and damping (Beck and Jennings 1980). This modal minimization routine has been proven to be superior to the transfer function approach in structural identification of linear models (Beck and Beck 1985). Additional background information regarding MODE-ID method can be found in EERL Reports 85-06 (Beck and Beck 1985) and 78-01 (Beck 1978). Information regarding the usage of MODE-ID can be found on the COMET website and a downloadable MODE-ID user manual (Beck and Mitrani 2003).

4.3 Results

The MODE-ID results shown here focus on the 2004 data obtained from the Parkfield school building and the Templeton hospital building. Older earthquake data will also be analyzed to ensure that changes in dynamic characteristics are not due to any discrepancies in MODE-ID settings. Previous results (Camelo, Beck and Hall 2002) will be used as reference to validate the results from older earthquakes.

4.3.1 Parkfield School Building

The Parkfield school building is only one story tall. It is expected that the dominant response will largely consist of the fundamental N-S, E-W modes and possibly one torsional mode. The frequency, damping and modeshape estimates are presented in Table 4-1 and Figure 4.1. In addition to the 2004 Parkfield Earthquake, records from two smaller earthquakes in 1993 and 1994 can be used to evaluate the change in dynamic characteristics over a range of ground motion amplitudes. Note from Figure 4.1 that the modes are coupled and therefore not purely N-S, E-W and torsional.

Table 4-1: The Parkfield school building frequency and damping estimates calculated from MODE-ID. The peak structural acceleration is provided for each earthquake.

Earthquake	Freq.(Hz) E-W	Damp. (%) E-W	Freq.(Hz) N-S	Damp. (%) N-S	Freq.(Hz) T	Damp. (%) T
4.2 M 0.123 g 04/04/1993	**7.3**	**12**	**8.6**	**15**	**11**	**16**
4.7 M 0.201 g 12/20/1994	**6.5**	**11**	**8.2**	**15**	**11**	**23**
6.0 M 0.30 g 09/28/2004	**5.3**	**13**	**6.0**	**22**	**8.9**	**13**

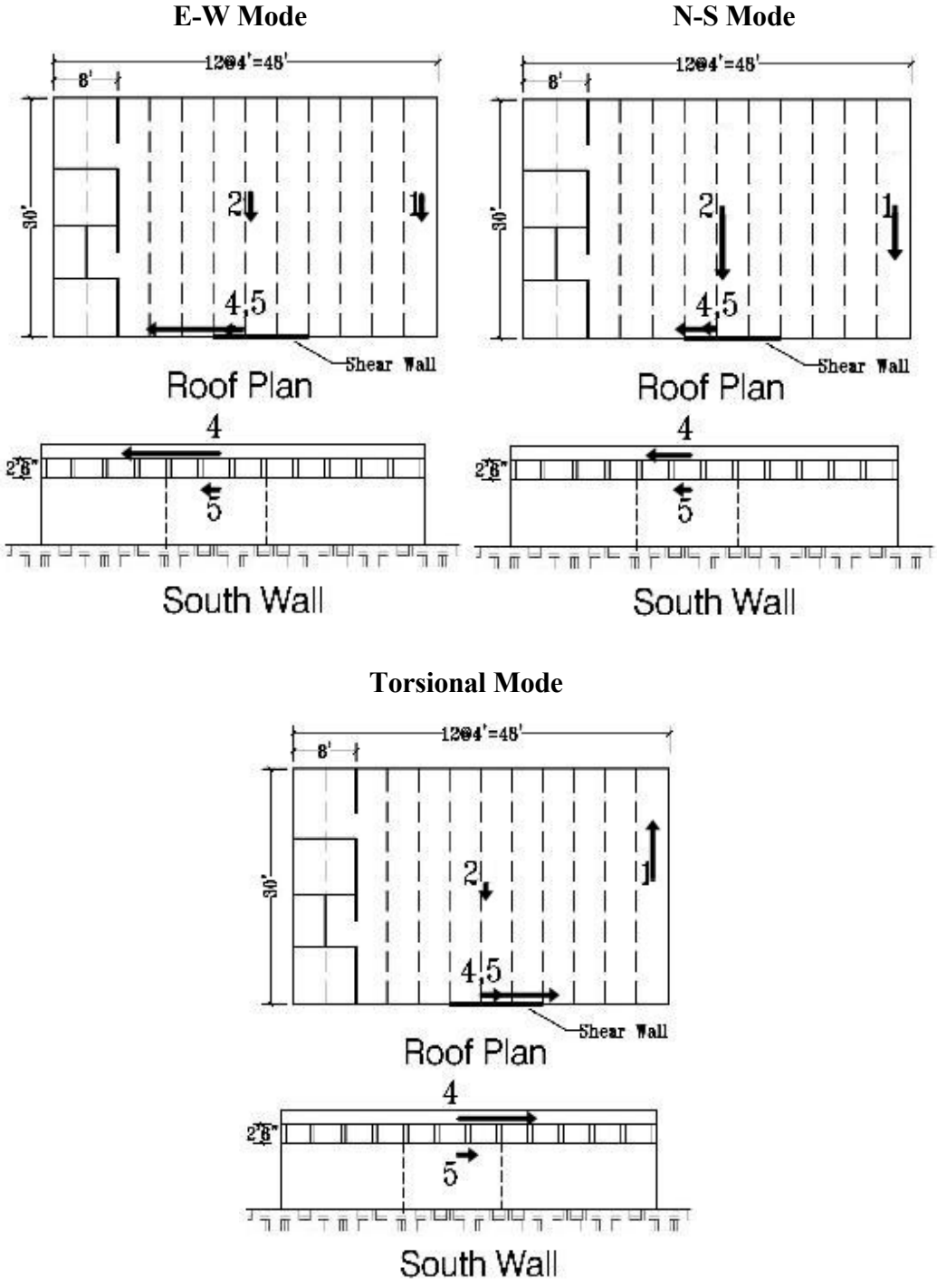

Figure 4.1: First three modeshapes of the Parkfield school building generated from the 2004 Parkfield Earthquake.

The 1993 and 1994 earthquakes have been re-analyzed and compared to the results in CUREE Task 1.3.3 (Camelo, Beck and Hall 2002). The values are found to be consistent. Since the magnitudes of the 1993 and 1994 earthquakes were similar, the reported modal frequency and damping estimates are comparable with the exception of the damping ratios of the torsional mode. The reason for this difference is not evident. It is likely the ground motion was not able to excite the torsional mode throughout the entire time record. In comparison with the records from 2004, amplitude dependence can be observed. The larger response amplitudes in 2004 are accompanied by lower frequencies and higher damping values.

Analysis of full-duration records produced high damping estimates as have been noted in previous studies. Damping is inherently difficult to estimate accurately with any method (Beck and Beck 1985). The credibility of a 20% damping ratio in wood-frame buildings needs to be investigated since steel or concrete buildings generally have values of 3 to 5%. For MODE-ID, a linear viscous damping is assumed. The meaning of a linear damping value that is fit under conditions of nonlinear response will be discussed in Chapter 5.

Table 4-1 also shows that the damping estimates in the N-S modes are generally greater than those of the E-W modes. This may be related to the fact that the north and south walls have less shear wall contribution due to a substantial area designated for windows, as shown in Figure 3.6.

Based on the identified modal parameters, MODE-ID can generate predicted responses for each of the measured channels. Table 4-2 displays the sum squared error between the measured and predicted responses from the different Parkfield school records.

It is evident that a two-mode MODE-ID model provides a drastic improvement compared to a single-mode MODE-ID model. This makes physical sense since it is anticipated that the fundamental frequencies in the longitudinal and transverse direction will be excited. The third mode, potentially a torsional mode, provides marginal improvement.

Figure 4.2 through Figure 4.10 present the predicted responses based on MODE-ID modal parameters for the measured earthquake records of the Parkfield school building in 1993, 1994, and 2004. Each earthquake record set has three MODE-ID models identified. Each model represents different number of modal modes used in the modal identification process. The red dotted lines are the measured responses and the blue lines are MODE-ID's predicted responses. The sum squared error is listed above each channel of record for comparisons between models. The two-mode model does a remarkable job in fitting the measured responses with the exception of the last channel, which sits on a shear wall.

Table 4-2: Sum squared error between the measured and predicted responses from different MODE-ID models. Measurements are from the 1993, 1994, and 2004 Parkfield school records.

Number of Modes	1993	1994	2004
One-Mode	0.4892	1.9049	4.5085
Two-Mode	0.1385	0.5383	1.8090
Three-Mode	0.1244	0.4599	1.5398

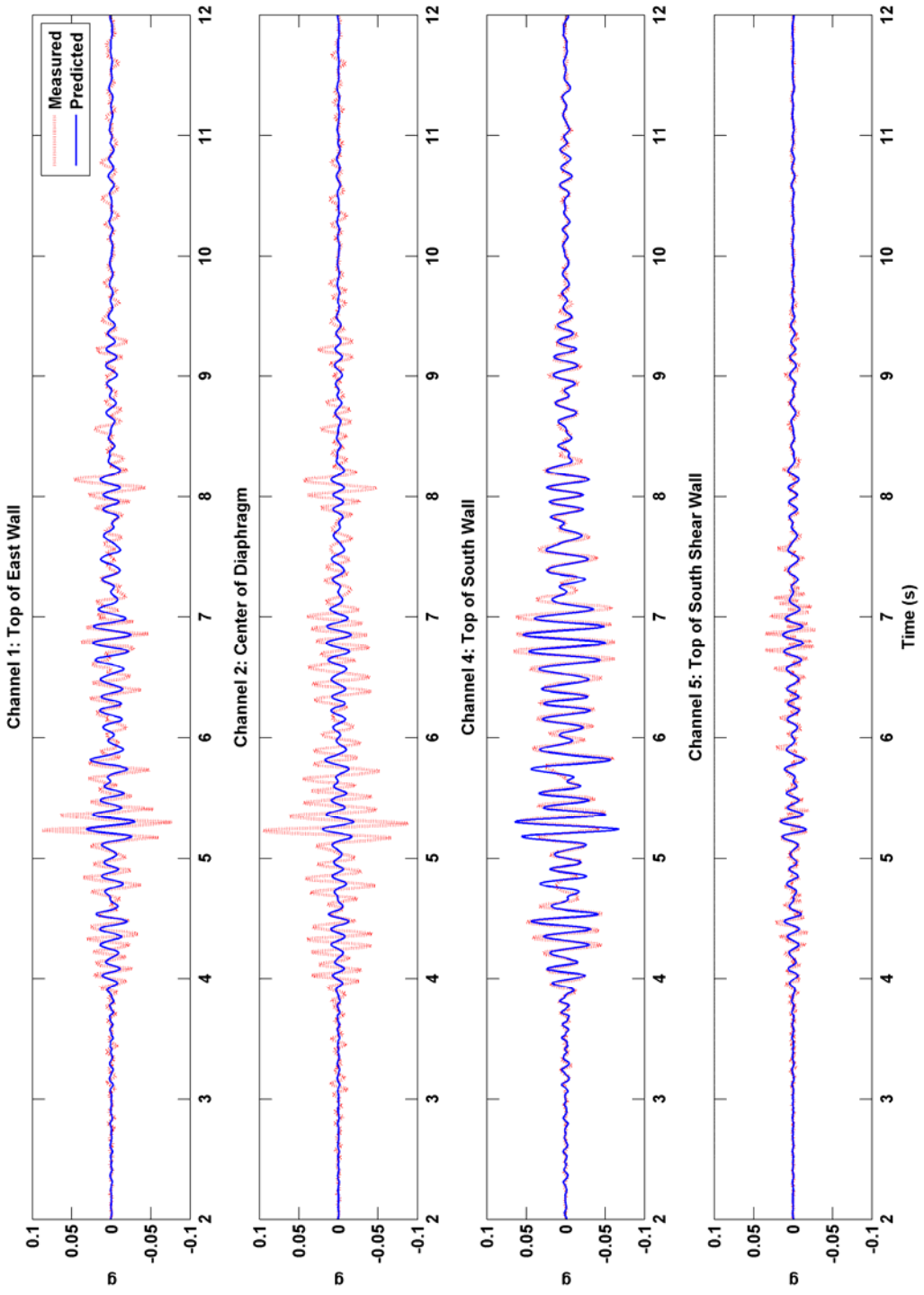

Figure 4.2: One-mode model for the 1993 Parkfield school records.

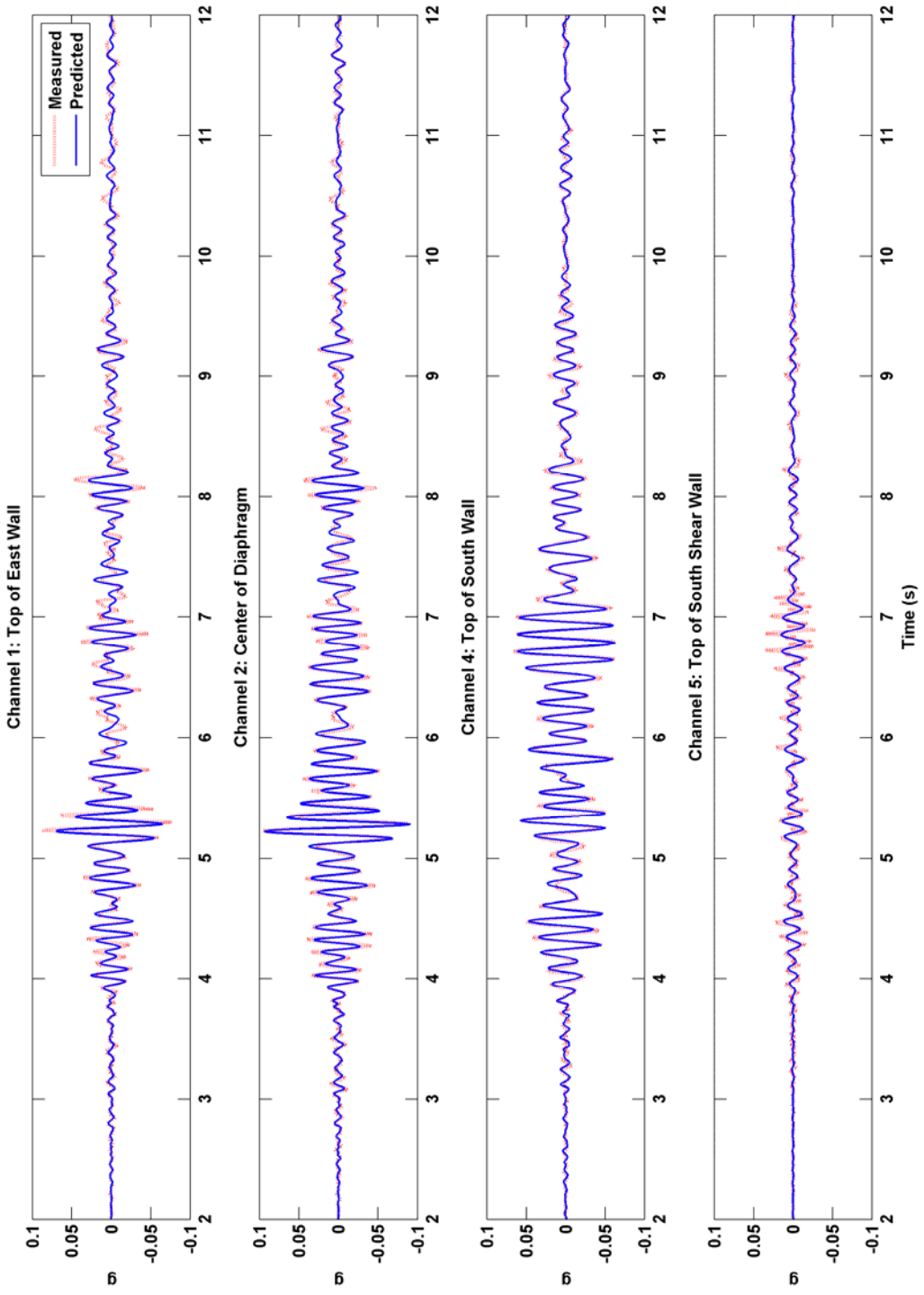

Figure 4.3: Two-mode model for the 1993 Parkfield school records.

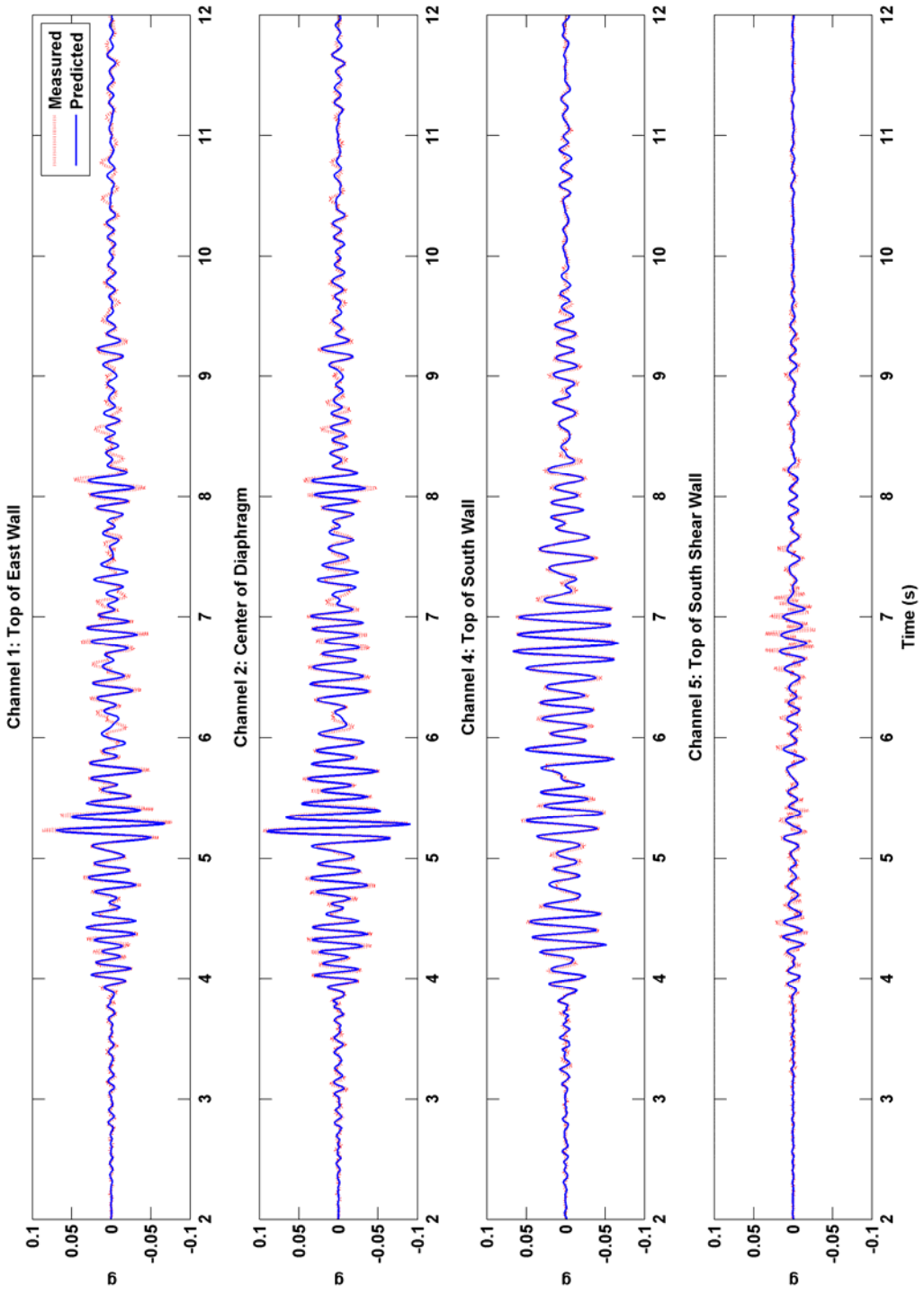

Figure 4.4: Three-mode model for the 1993 Parkfield school records.

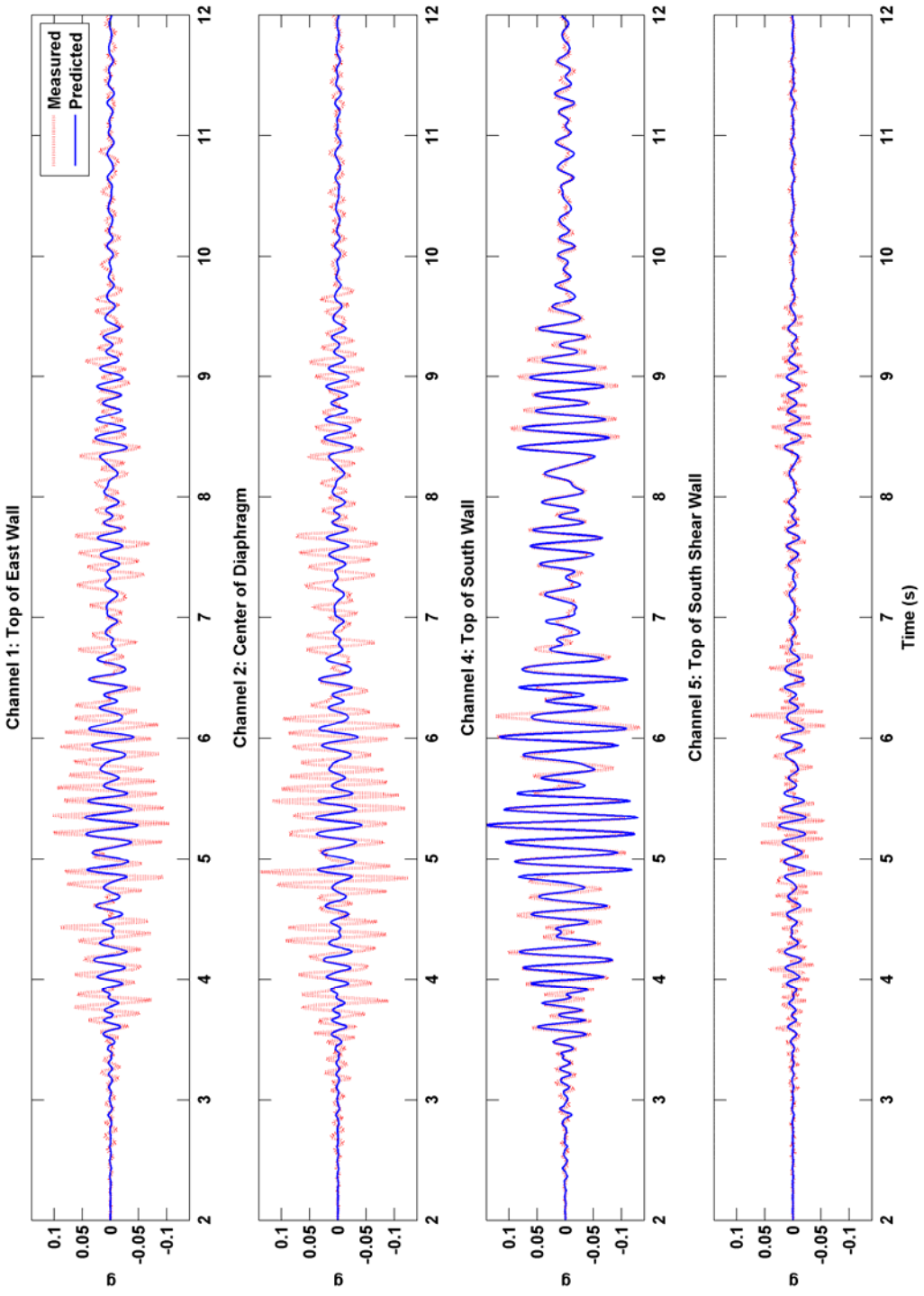

Figure 4.5: One-mode model for the 1994 Parkfield school records.

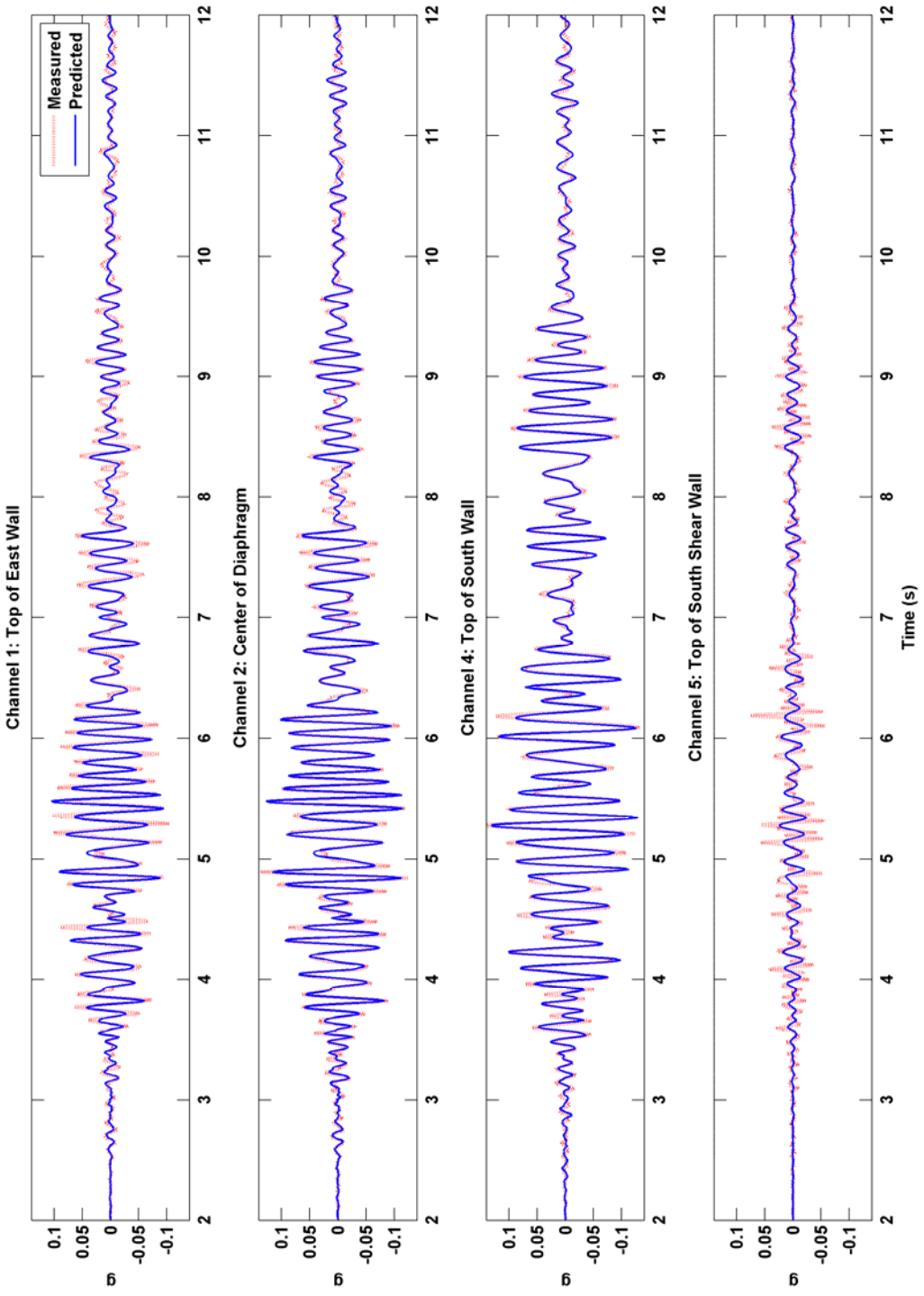

Figure 4.6: Two-mode model for the 1994 Parkfield school records.

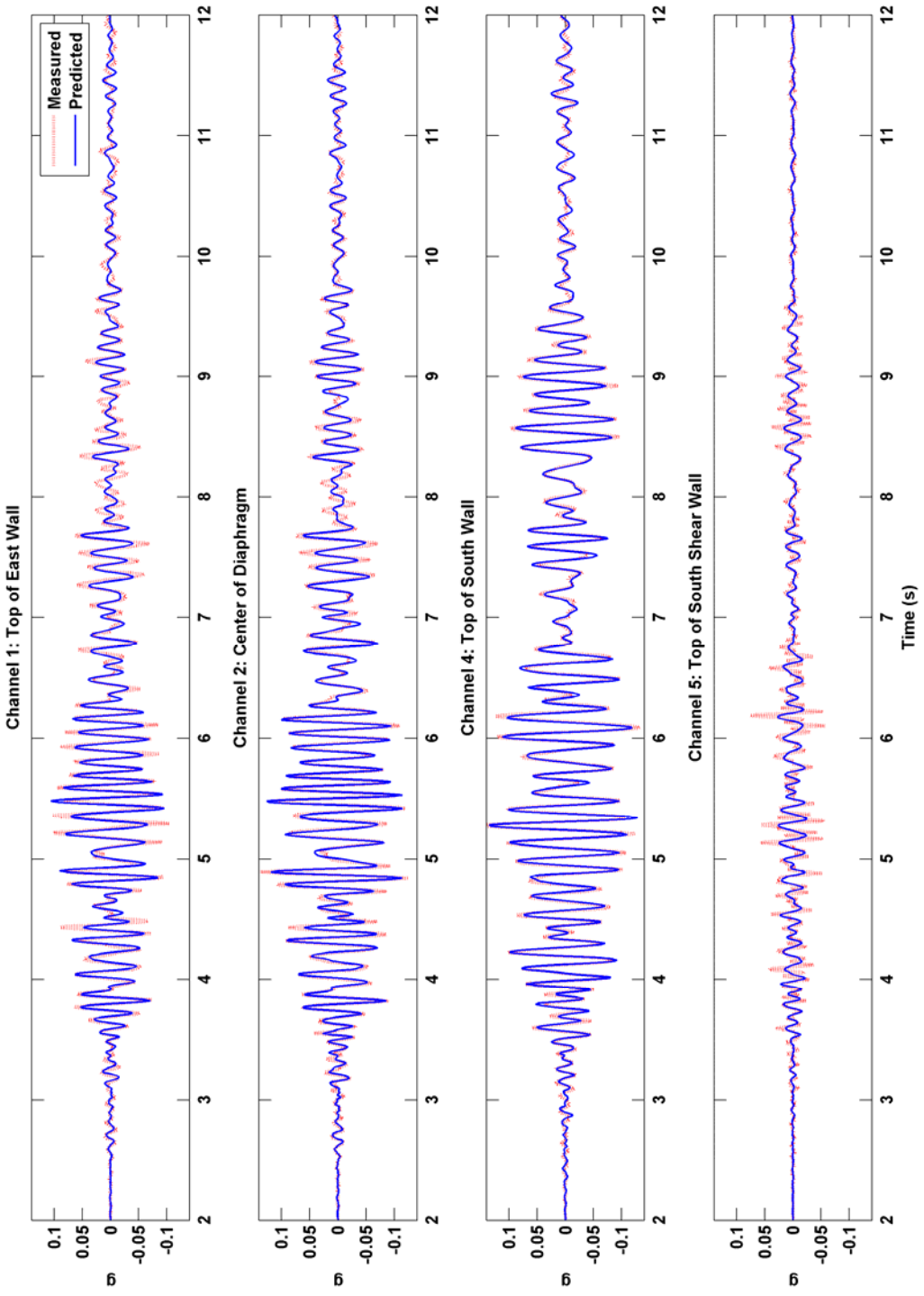

Figure 4.7: Three-mode model for the 1994 Parkfield school records.

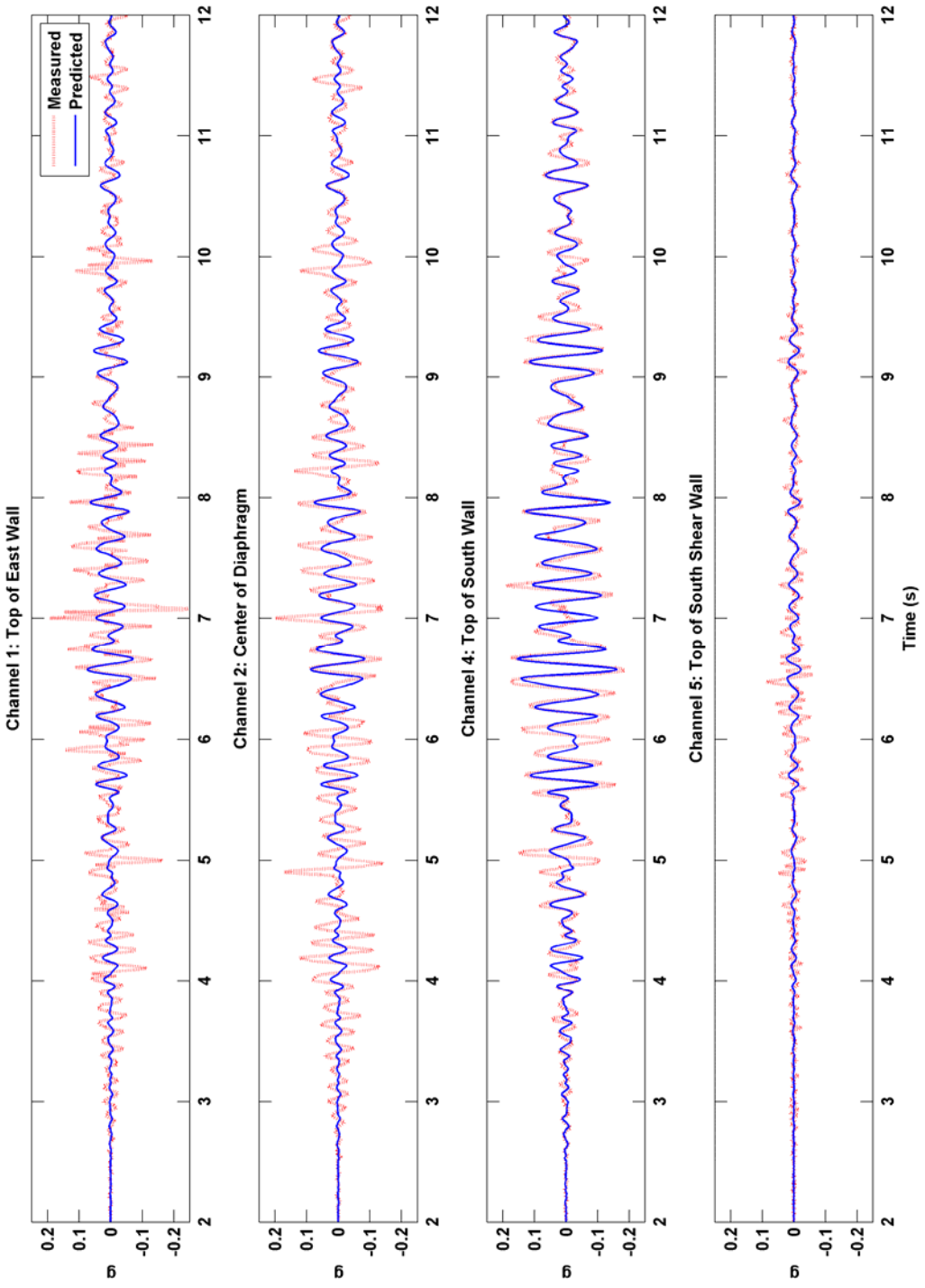

Figure 4.8: One-mode model for the 2004 Parkfield school records.

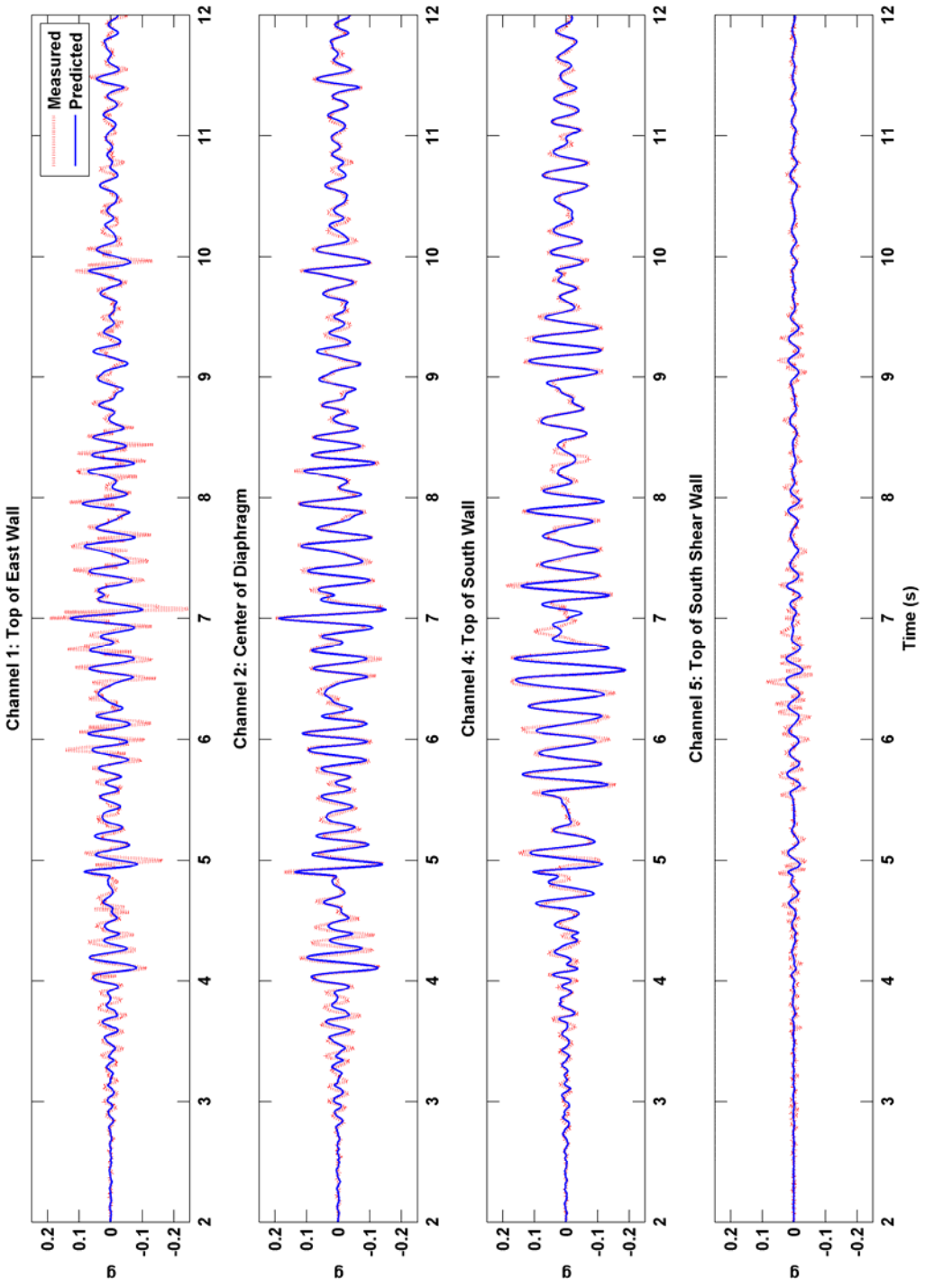

Figure 4.9: Two-mode model for the 2004 Parkfield school records.

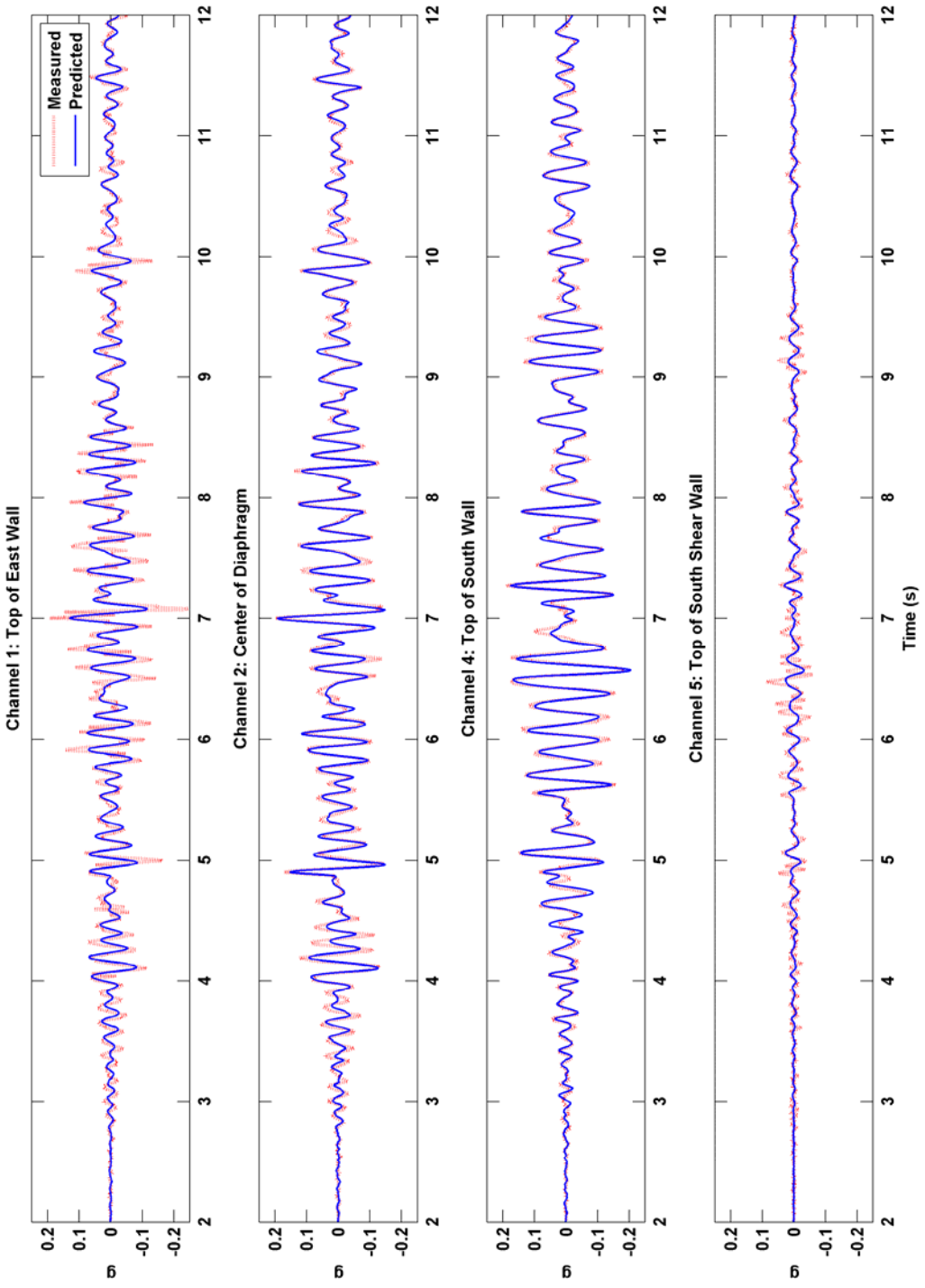

Figure 4.10: Three-mode model for the 2004 Parkfield school records.

A windowing analysis can be performed on the 2004 Parkfield records through MODE-ID. Results are presented in Figure 4.11 and Figure 4.12. A two-second window with 50% overlap was chosen because it is the smallest window that results in consistent convergence. Windowing analysis reveals the change in modal frequency and damping during the earthquake.

From Figure 4.11 it is apparent that the building did reach nonlinear motion because each fundamental frequency changed during the course of the response. Following the locus of the estimated fundamental frequencies of the building, the initial frequencies were around the 7 Hz range when the initial motion was recorded. The building's frequencies decrease to nearly 5 Hz as the magnitude of the ground response increases, reaching these significantly lower values during the time of the strongest ground shaking at around 5 seconds (Figure 3.7). As the ground motion subsides, the building's fundamental characteristics revert to initial frequencies. This suggests that the building sustained no significant damage.

The window analysis on damping estimates (Figure 4.12) shows that damping fluctuates greatly throughout the earthquake shaking. At lower ground motions, the damping ratio still displays values of 12-20%, which are high relative to steel and concrete buildings. These results are a fabrication of MODE-ID attributing high damping estimates to compensate for the high participation factors for low amplitude responses. There is a trend that the frequency estimates decrease and damping estimates increase before the largest amplitude of ground motion. How early the trend begins depend on the length of window used.

This should not be seen as an error, but a tradeoff between model resolution and accuracy. Additionally, as ground motion subsides, the reported damping estimates have high variance in a small window time frame. To illustrate this, longer time windows were used for records from 1993 and 1994 Earthquakes (Figure 4.13 to Figure 4.16). The fluctuations in damping estimates are no longer present at the expense of a coarser time resolution. The same observations can be made with regard to the amplitude dependence of frequency and damping estimates.

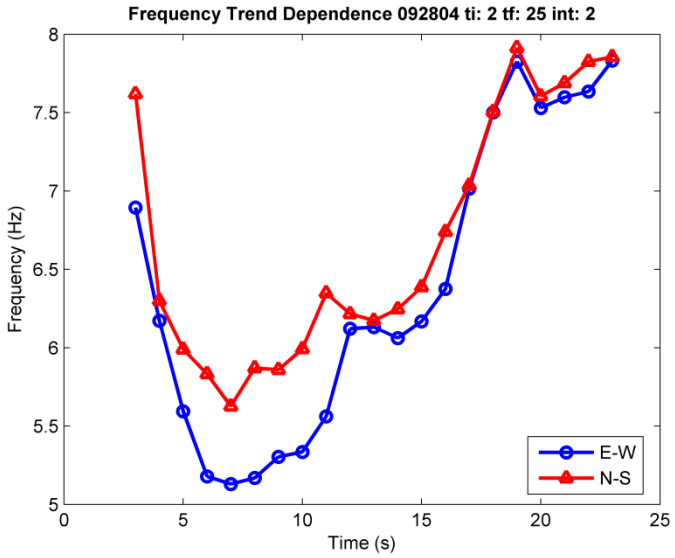

Figure 4.11: Amplitude dependence of the E-W and N-S mode frequency estimates for the Parkfield school building. The window analysis is performed on the 2004 Parkfield Earthquake.

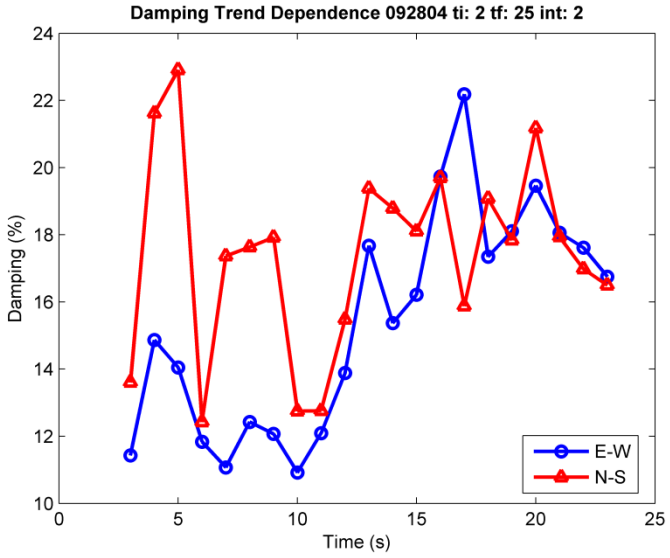

Figure 4.12: Amplitude dependence of the E-W and N-S mode damping estimates for the Parkfield school building. The window analysis is performed on the 2004 Parkfield Earthquake.

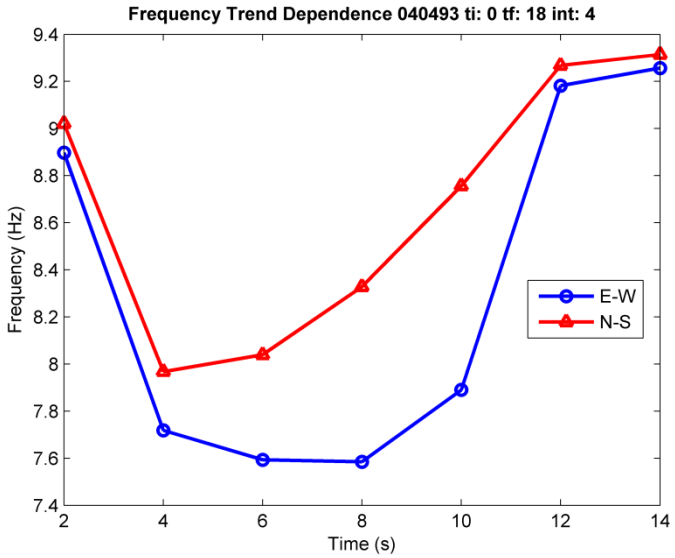

Figure 4.13: Amplitude dependence of the E-W and N-S mode frequency estimates for the Parkfield school building. The window analysis is performed on the 1993 Parkfield Earthquake.

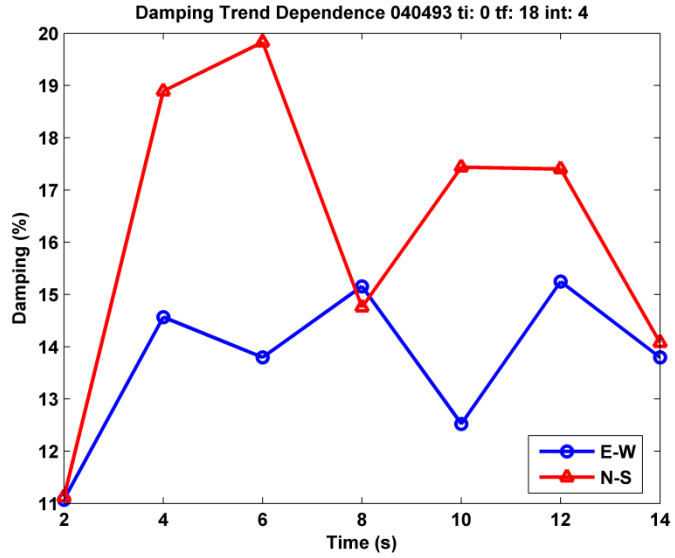

Figure 4.14: Amplitude dependence of the E-W and N-S mode damping estimates for the Parkfield school building. The window analysis is performed on the 1993 Parkfield Earthquake.

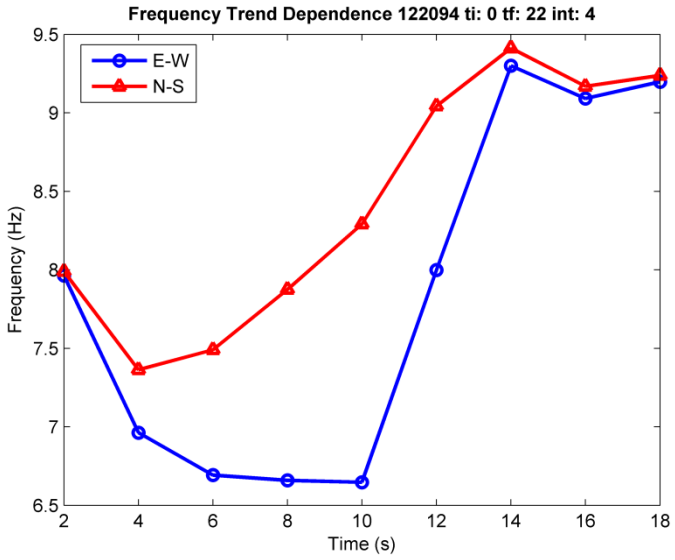

Figure 4.15: Amplitude dependence of the E-W and N-S mode frequency estimates for the Parkfield school building. The window analysis is performed on the 1994 Parkfield Earthquake.

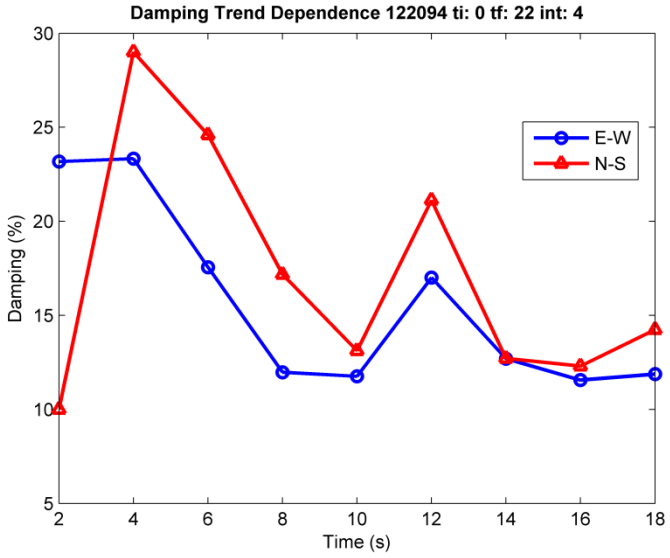

Figure 4.16: Amplitude dependence of the E-W and N-S mode damping estimates for the Parkfield school building. The window analysis is performed on the 1994 Parkfield Earthquake.

4.3.2 Templeton Hospital

Frequency, damping and modeshape estimates are presented in Table 4-3 and Figure 4.17. The first mode mostly involves transverse motions of the west wing, and the second mode is predominately north wing. Both wings contribute to the third mode. The instrumentation layout allows only the study of the northwestern wings of this very asymmetric building.

Table 4-3 contains the results for the M 6.5 earthquake in 2003, three of its aftershocks, and another smaller earthquake in 2005. Results seem to be consistent with the observations made from the analysis of the Parkfield school building. Reported frequencies are higher for the aftershock records and much lower for the 6.5 M San Simeon Earthquake. Damping estimates continue to be within the 15-20% range with the west wing exhibiting higher damping for all five records.

Figure 4.18 to Figure 4.20 are the predicted responses generated from MODE-ID for the 2003 Templeton hospital records. Again, the sum squared error is labeled above each channel. For the 2003 record, the one-mode model had a sum squared error of 61.584 compared to 28.4894 and 20.8913 for the two- and three-mode model. Larger discrepancies are seen in rows 1, 4, and 6, which correspond to measurement channels 4, 7, and 9 in the instrumentation layout. These channels sit along the outer shear walls.

Table 4-3: Templeton hospital building frequency and damping estimates calculated from MODE-ID. The peak structural acceleration is provided for each earthquake.

Earthquake	Freq. (Hz) W. Wing	Damp. (%) W. Wing	Freq. (Hz) N. Wing	Damp. (%) N. Wing	Freq. (Hz) Mode 3	Damp. (%) Mode 3
4.4 M .017 g 05/16/05	**7.3**	**20**	**7.0**	**12**	**9.9**	**8.9**
Aftershock .031g 02/09/04	**7.4**	**22**	**7.3**	**15**	**9.7**	**21**
Aftershock .073g 05/02/04	**6.8**	**18**	**6.7**	**15**	**9.2**	**11**
Aftershock .217 g 10/02/04	**6.5**	**19**	**5.8**	**16**	**8.1**	**15**
6.5 M 1.3 g 12/22/03	**5.0**	**17**	**4.8**	**16**	**7.2**	**19**

West Wing Mode **North Wing Mode**

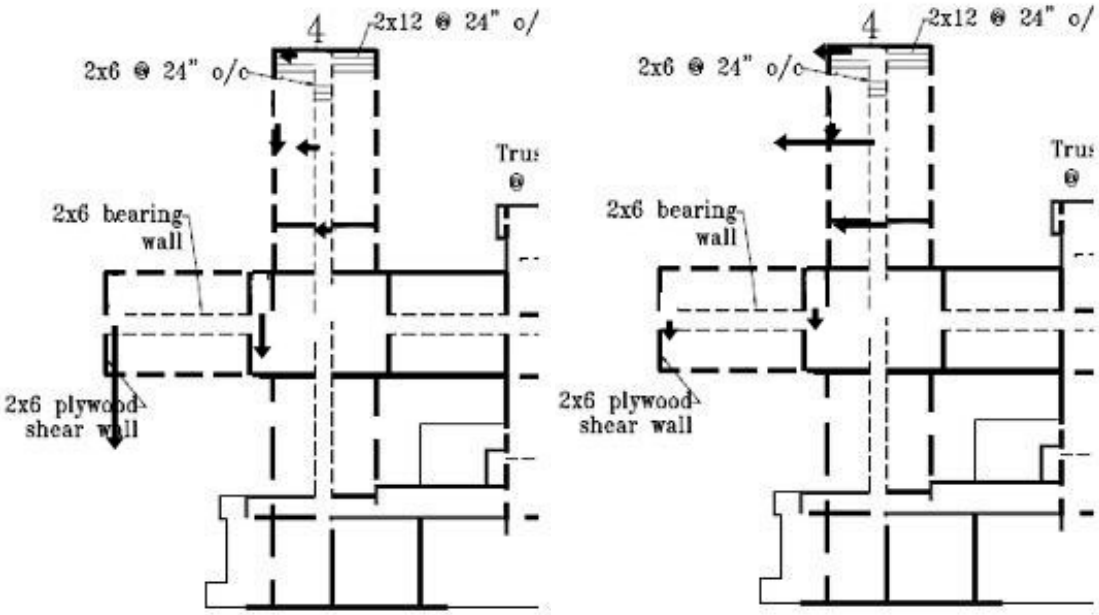

Mode 3

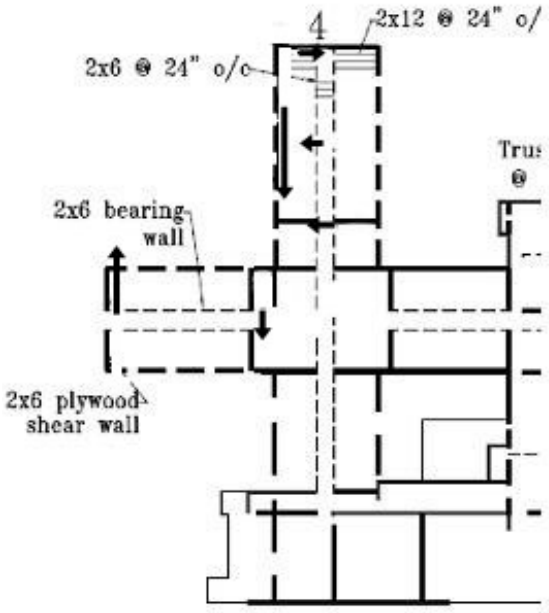

Figure 4.17: First three modeshapes of the Templeton hospital building generated from the 2003 San Simeon Earthquake.

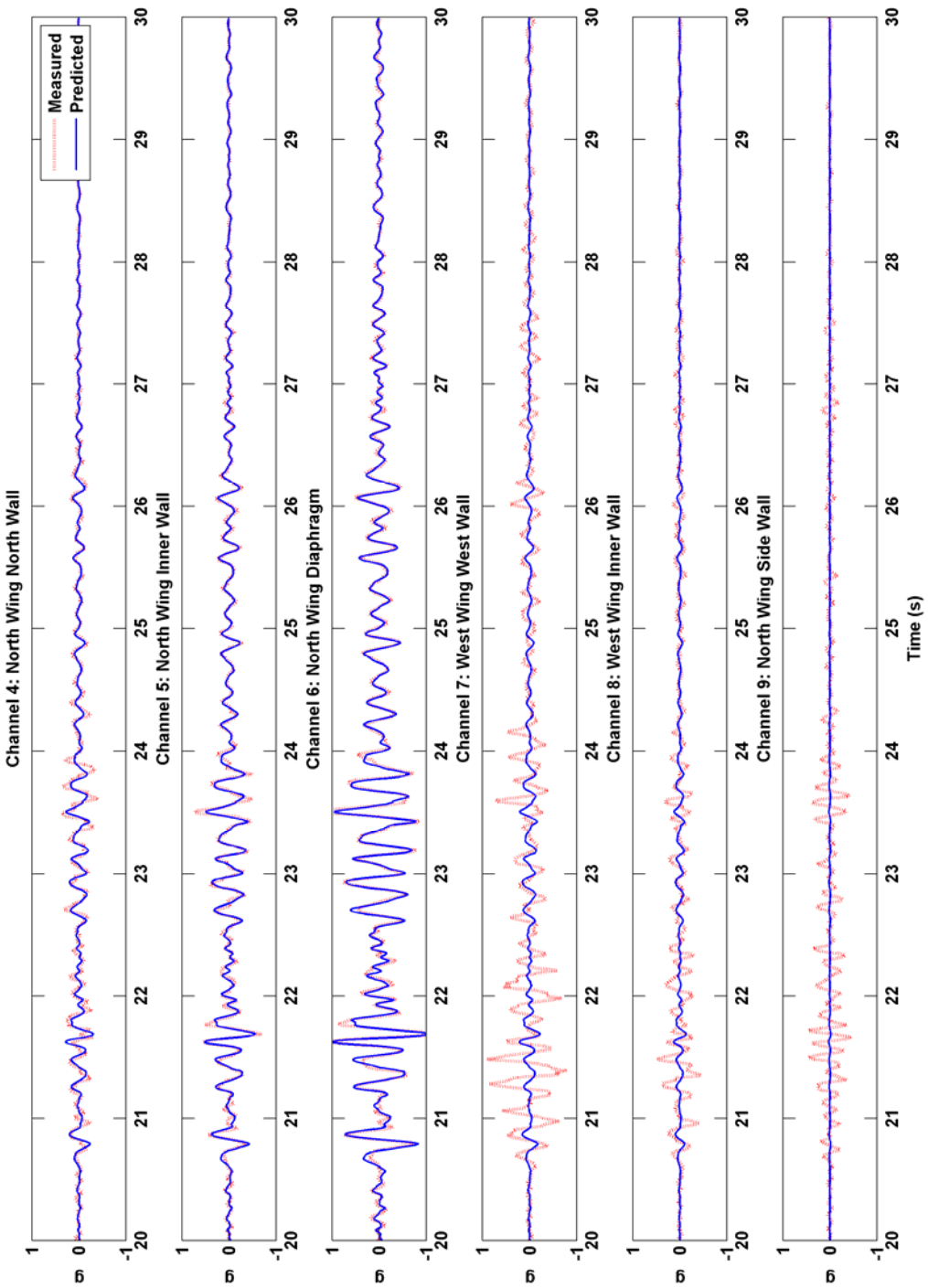

Figure 4.18: One-mode model for the 2003 Templeton hospital records.

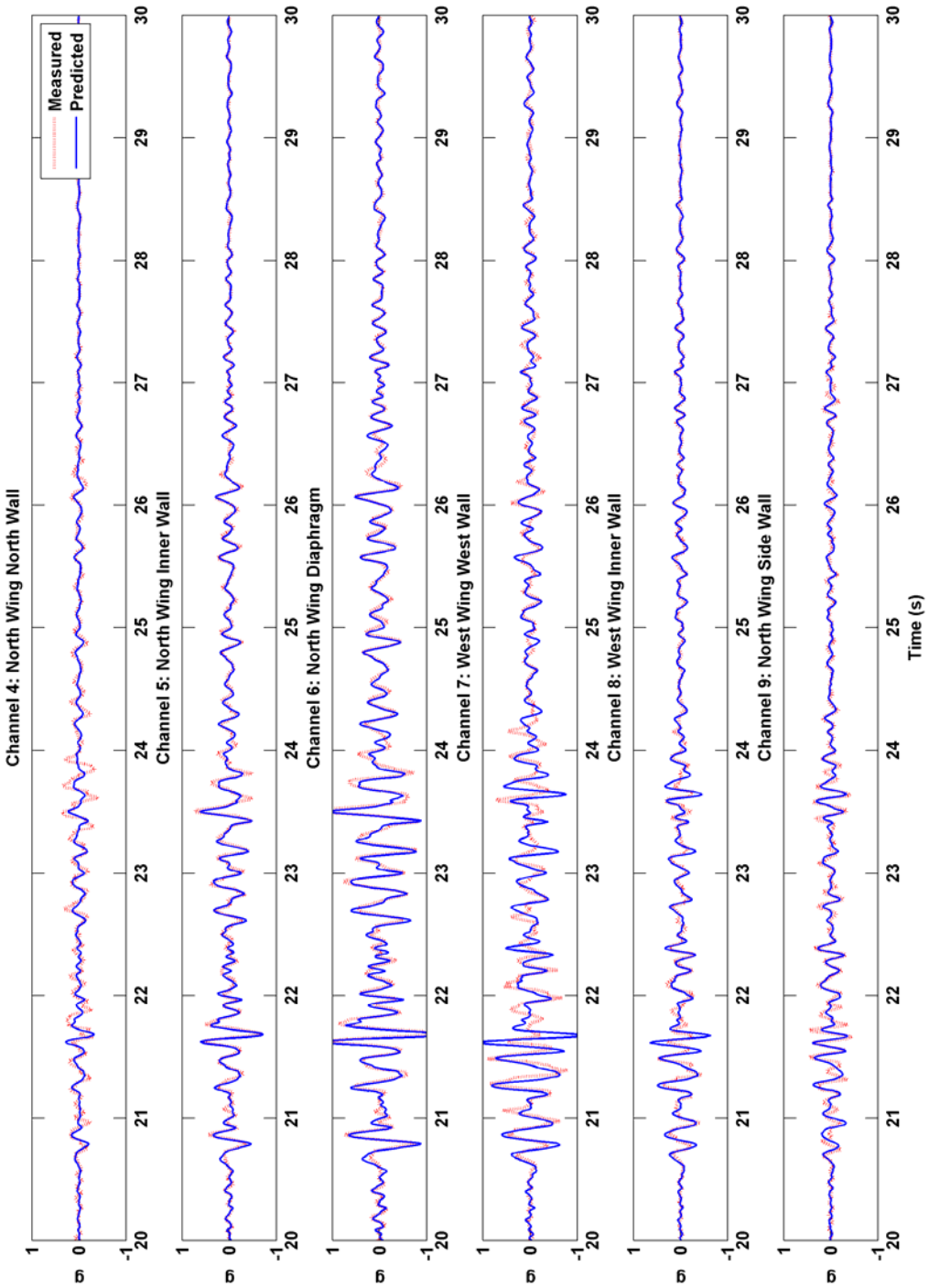

Figure 4.19: Two-mode model for the 2003 Templeton hospital records.

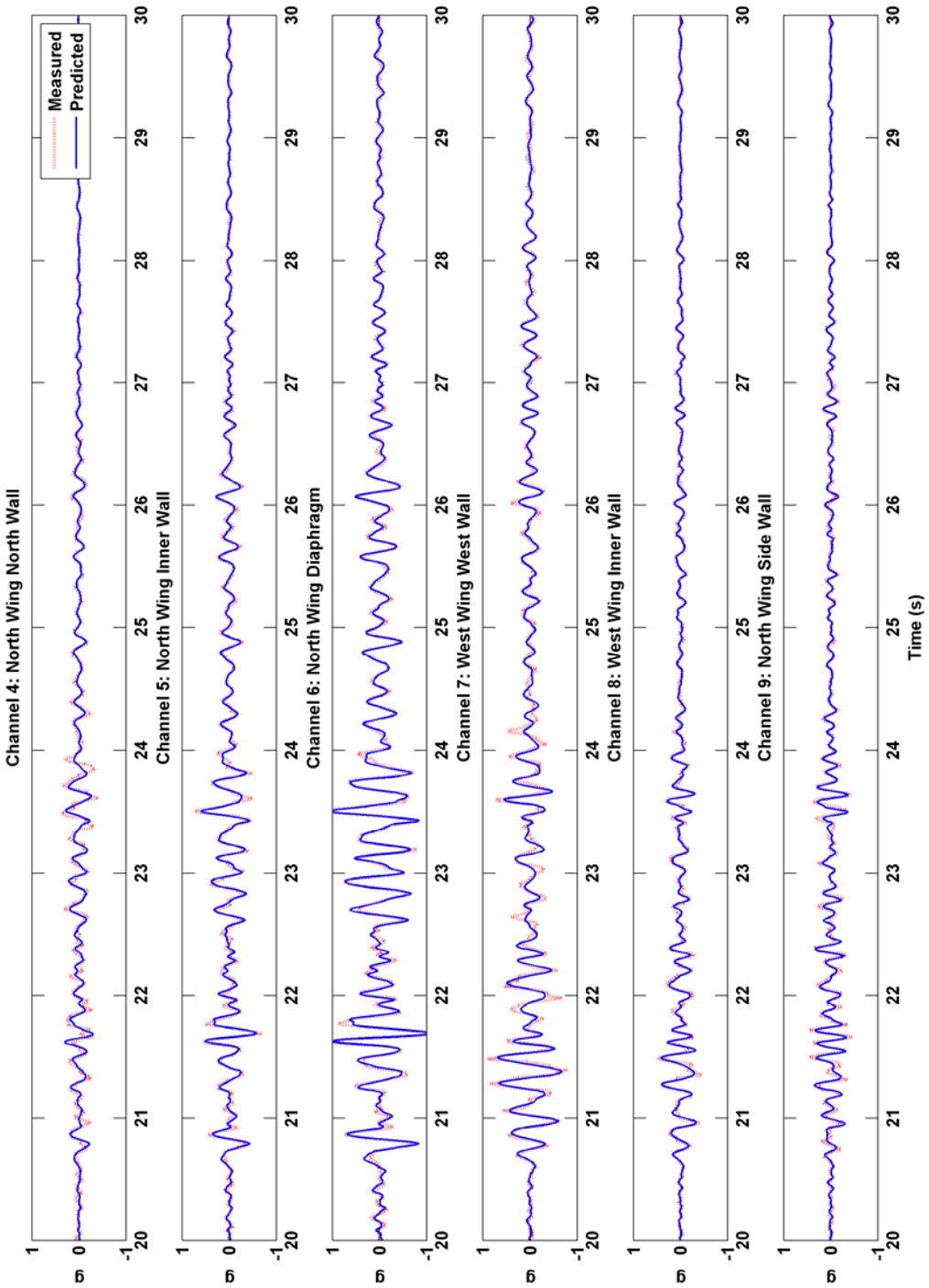

Figure 4.20: Three-mode model for the 2003 Templeton hospital records.

Window analysis was also performed on the Templeton hospital records. The amplitude dependence of the modal parameters is shown in Figure 4.21 through Figure 4.24. Refer to Figure 3.11 and Figure 3.12 for the acceleration time histories of the 2003 San Simeon Earthquake. The locus of frequency estimates in Figure 4.21 demonstrates the nonlinear response during the earthquake. The fundamental frequencies lost up to 50% of their initial values during the peak of the ground motion. These frequencies do return close to their initial values about 50 to 60 seconds into the record (not shown in figure).

The trend of high damping estimates at peak ground motion seen in the Parkfield school building is consistent with the Templeton hospital record (Figure 4.22). The high damping estimate is compensating for the dissipation of energy through nonlinear responses. Details of the energy dissipation are discussed in the next chapter. Figure 4.23 and Figure 4.24 show the windowed analysis for the 2004 San Simeon aftershock. Again the plots support many of the observations made in earlier sections.

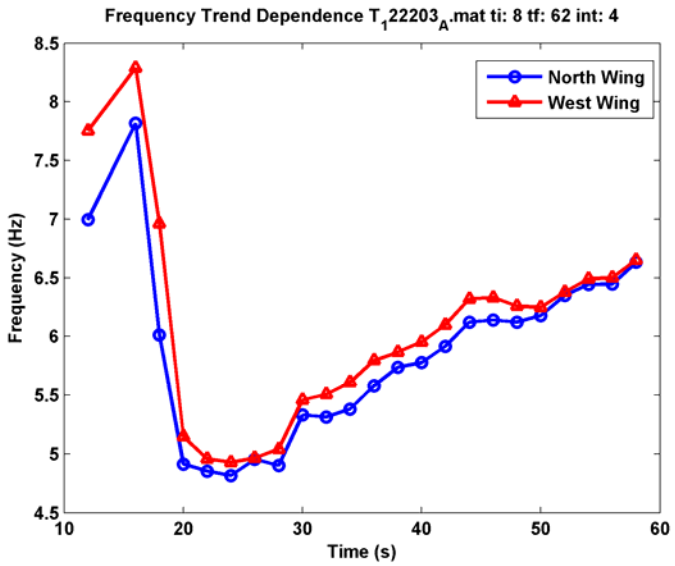

Figure 4.21: Amplitude dependence of the west wing and north wing frequency estimates for Templeton hospital building. The window analysis is performed on the 2003 San Simeon Earthquake.

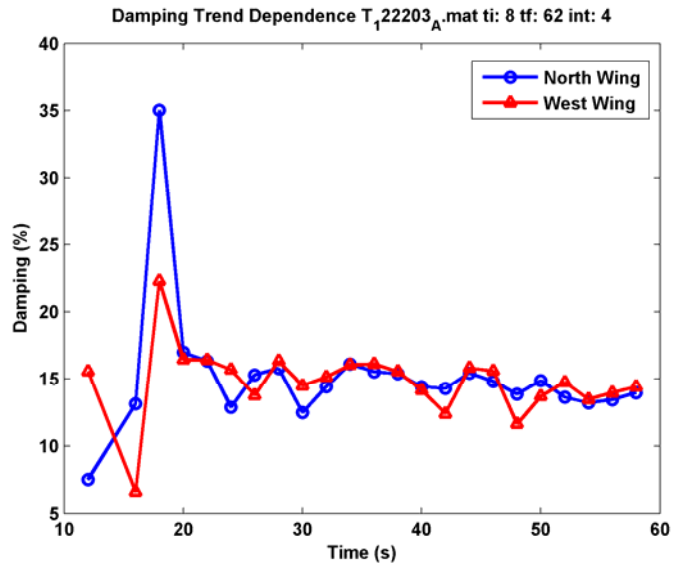

Figure 4.22: Amplitude dependence of the west wing and north wing mode damping estimates for Templeton hospital building. The window analysis is performed on the 2003 San Simeon Earthquake.

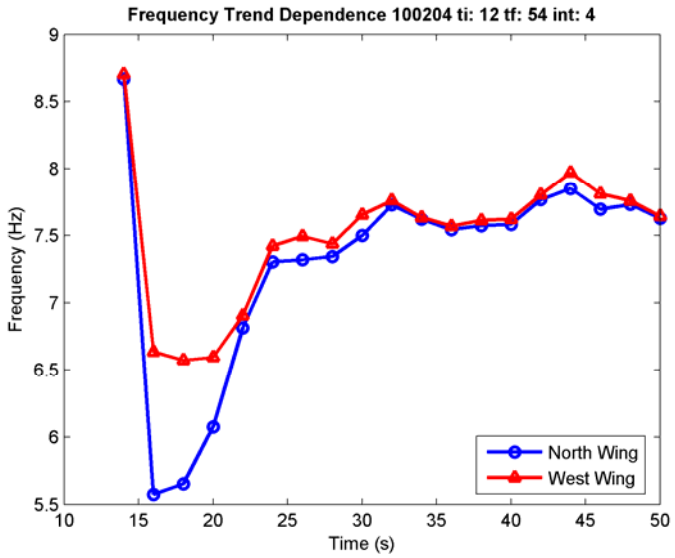

Figure 4.23: Amplitude dependence of the west wing and north wing frequency estimates for Templeton hospital building. The window analysis is performed on the 2004 San Simeon aftershock.

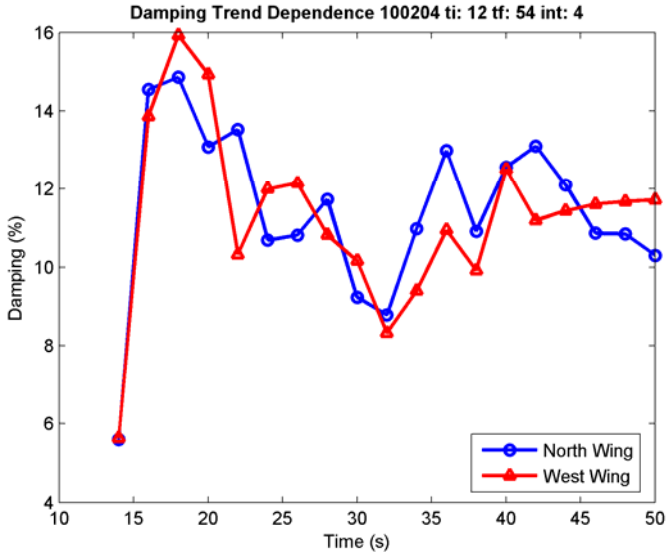

Figure 4.24: Amplitude dependence of the west wing and north wing mode damping estimates for Templeton hospital building. The window analysis is performed on the 2004 San Simeon aftershock.

4.4 Conclusions

Analyses of the 2004 Parkfield and 2003 San Simeon Earthquakes and some aftershocks reaffirm many of the claims of amplitude dependence of modal parameters. The 2-4 second time windows with 50% overlap offer greater insight into the progression of the estimates through time than previous studies. Predicted responses from MODE-ID greatly resembled the measured responses. The largest discrepancies are seen on measurement channels that are located on shear walls. The accelerations are smaller at these locations, and the differences are more pronounced with the magnified scale. The identified modal parameters in this chapter will be a basis in interpreting the physical behavior, primarily hysteretic responses, of the wood-frame structure in a later chapter.